

# HYDRO-MECHANICAL COUPLING IN THE BOOM CLAY (MOL URL, BELGIUM): RECENT IN-SITU OBSERVATIONS, PREDICTIONS AND PERSPECTIVES

Jean-Dominique BARNICHON and Geert VOLCKAERT  
SCK•CEN (Belgian Nuclear Research Centre), Boeretang 200 - 2400 Mol, Belgium

## Abstract

The Boom Clay is considered as a candidate host-rock for the Belgian disposal of radioactive waste. Thanks to the recent sinking of a new shaft to extend the underground laboratory at the Mol site, new in-situ data have been obtained. They consist in the observation of an important fracturing evidenced during the excavation of the shaft annexes and in well-correlated hydraulic perturbations in the far field (maximum of 0.2 MPa at 60 m radius). These observations cannot be explained from simple poroplastic models that predict a maximum perturbation extent of 25 m under full deconfinement. Thus, increasingly more complex models are built to explain this discrepancy. It is proposed that the low support pressure imposed by the primary lining, combined with the large time over which this support condition held, has favoured the decompression of the clay massif through differed effects, mainly skeleton viscosity. This resulted in fracturing in the near field, leading to an apparent increase of the excavated radius and to a hydraulic perturbation in the far field. This interpretation still needs to be validated/invalidated with future data (available next year). The effects on the overall performance of the repository should remain limited due to self-healing.

## 1. Introduction

In the framework of the underground storage for high level radioactive waste, an accurate assessment of the perturbations induced by the excavation is important for design purpose, and may also have impact on the overall performance of the disposal. Generally, the excavation of a gallery induces perturbations of the surrounding in-situ stress ( $\sigma$ ) and pore pressure ( $u_w$ ), associated with displacements ( $u$ ). The observations gained during the excavation of the Test-Drift in the Boom Clay in 1987 showed a quite large extent of the associated hydraulic perturbation, which remained very difficult to explain (see e.g. Barnichon, 1998). Associated with the PRACLAY (PREliminARy demonstration test for CLAY disposal of high activity radioactive waste) project, the currently running extension of the Mol URL has allowed obtaining new in-situ observations and data. This motivated a synthesis of the observations and of their interpretation that are presented in this paper.

A review of the in-situ observations in the Boom Clay is first presented here in the light of these new data, focusing on the hydraulic disturbance and on the fracture observation. This choice is justified as the pore pressure measurement in the Boom Clay is usually accurate, and as it is very sensitive to mechanical variations (actually the volumetric part) through the strong hydro-mechanical coupling that exists in this material.

Then, the solutions obtained from the methods (analytical or numerical) that predict the hydro-mechanical response ( $\sigma$ ,  $u$  and  $u_w$  fields) of saturated porous media are used to estimate the perturbations that should theoretically be observed. Models with increasing complexity (time-independent and time-dependent) are considered to investigate the possible origins of the perturbations observed in-situ.

Finally, based on the observations and predictions, a global interpretation of the observed phenomena is proposed.

## 2. Observations from the Underground Research Laboratory

A view of the present-day underground installations at the Mol site is presented on Figure 1. Only the parts that have been excavated in the Boom Clay without ground freezing are considered in the following, i.e. the experimental shaft, the Test-Drift (excavated in 1987), the bottom part of the second shaft (excavated in 1998-99) and the starting chambers of the second shaft (excavated in 1999). Finally, the perturbations of the pore pressure field are presented.

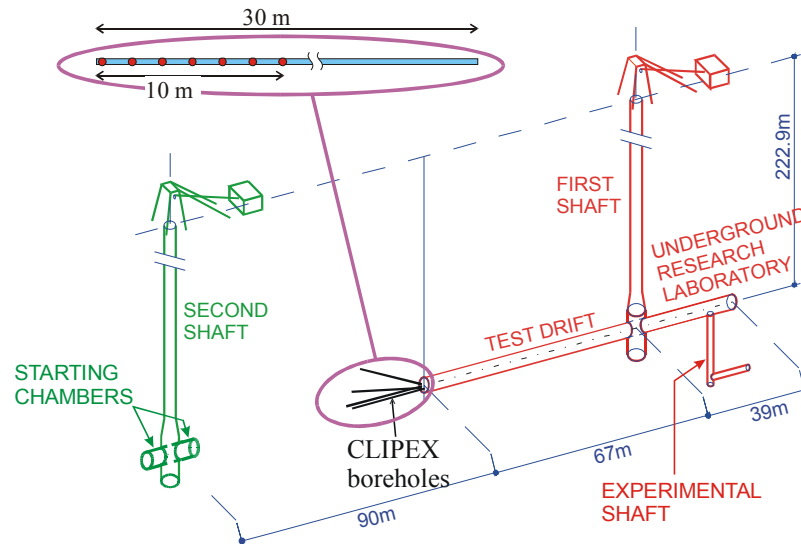


Fig.1. View of the underground installations in the Boom Clay at the Mol site.

### 2.1 The Test-Drift

The Test-Drift has been excavated from April 1987 from the first shaft (see Figure 1), with an excavated radius of about 2.45 m. Prior its excavation, instrumentation was placed in the clay massif, particularly piezometric filters that recorded the variation of pore pressure during the excavation. Details about the set-up can be found in Bonne et al. (1992). As one of the results, an important variation of pore pressure (up to 1 MPa) was measured at a radial distance of 12 m from the Test-Drift axis (see Figure 2). Given the low hydraulic conductivity ( $k = 4 \cdot 10^{-12}$  m/s) of the Boom Clay host-rock, the excavation is almost undrained. Thus the pore pressure variation must be correlated with the plastic zone around the excavation (as the variation of mean pressure is nil in the elastic zone, see e.g. Giraud, 1993). Thus, these data would argue for an extent of the plastic zone around the Test-Drift of at least 12 m. However, its is very difficult to predict these observations using classical plasticity models with the representative parameters for the Boom Clay. Efforts to use more realistic models, such as bounding surface plasticity models (Barnichon, 1998), were not fully satisfactory: the discrepancy between the observations and the results was still very large, though reduced compared to the classical plasticity models. Last, the predicted displacements were comparable with the measurements.

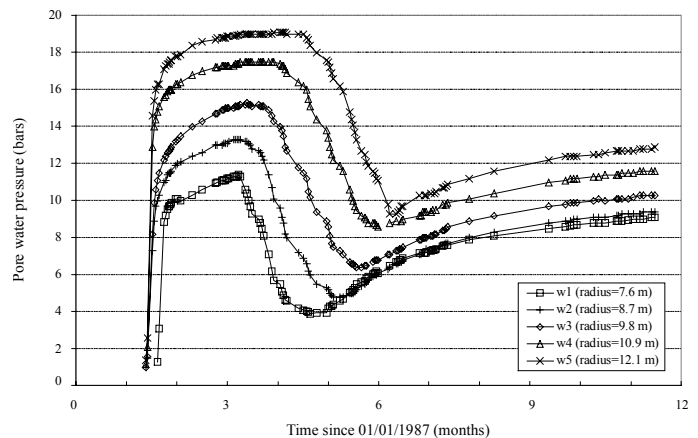


Fig.2. Pore pressure time-evolution during the Test-Drift excavation, adapted after (Bonne et al., 1992).

### 2.2 The bottom part of the second shaft

The second shaft has been excavated in 1998-99. In its bottom part (sunk in 1999), entirely located in the clay host-rock, it consists in an excavation with an internal radius  $r_i = 4$  m, which was primarily lined (from top to bottom) with sliding ribs (i.e. a relatively soft lining). After completion of the excavation, a secondary rigid lining (reinforced cast concrete) was placed from the bottom. The time span between the placement of the primary and secondary lining was around two months, which allowed an important convergence of the clay. During the excavation of the shaft foundation in the clay, some fracturing has been observed, such as shown on Figure 3 (indicated by the arrows).



Fig.3. Photograph of a fracture surface in the foundation enlargement of the second shaft.

### 2.3 The starting chambers

From the bottom of the second shaft, the two opposite starting



Fig. 4. View of the fracture surface in the South starting chamber (the thick black curves visualise the trace of horizontal planes on the fracture surface).



Fig. 5. Traces of the fractures (indicated by the black arrows) in the lateral wall of the South starting chamber.

chambers have mainly been excavated between the 16<sup>th</sup> March and the 16<sup>th</sup> April 1999. These works led to front stability problems resulting from well developed fracturing of the clay host-rock close to the excavation. This fracturing appeared as large fracture surfaces visible at the front of each starting chamber (see Figure 4). Importantly, they showed very clear indicators of movements indicating a radial sliding, and an axial symmetry around the main shaft axis. The fracturing also appeared as fracture traces in the lateral walls of the starting chambers (see Figure 5). A key point is to realise that these two starting chambers cross-cut the plastic zone generated by the excavation of the main shaft along its radial direction, consequently observed fractures could be related with the excavation of the first shaft. In any case, this interpretation is supported by the axial symmetry observed with respect to the axis of the shaft.

#### 2.4 The far field: CLIPEX instrumentation

Originally, the CLIPEX instrumentation—piezometric filters, total pressure sensors and displacement devices—(Bernier and Van Caueren, 1998) has been placed in 1998 in the Boom Clay to record the effects of the excavation of the connecting gallery from the second shaft towards the Test-Drift (Figure 1). Interestingly, it evidenced the effects of

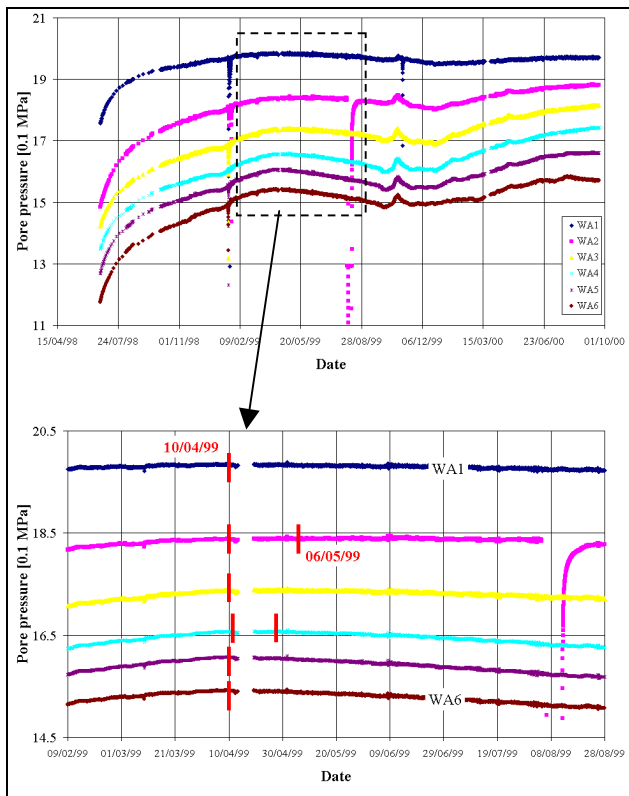


Fig. 6. Pore pressure recorded in borehole A2 (top), with details around the peak zone (bottom).

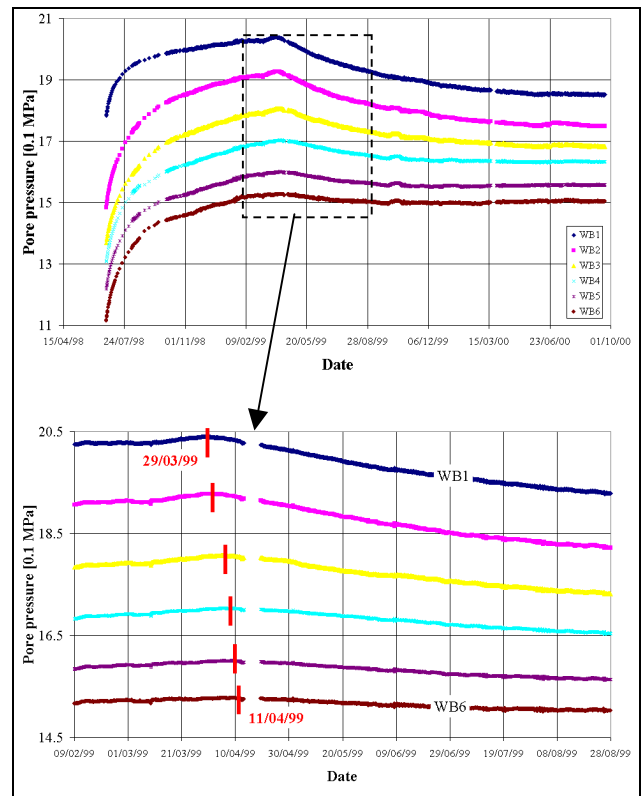


Fig. 7. Pore pressure recorded in borehole B2 (top), with details around the peak zone (bottom).

the second shaft excavation in the far field, particularly with the measurement of pore pressure. Results for the borehole A2 (oriented along the axis of the connecting gallery) and the borehole B2 (same direction than the gallery axis, but inclined 4 m upwards) are presented on Figures 6 and 7, respectively. Note that the filters of these two boreholes are located between 60 to 70 m from the axis of the second shaft (see Figure 1). Measurements of both A2 and B2 show somehow similarities in their time evolution. First, the pore pressure increases rapidly after emplacement of the measuring devices in the host-rock. This is followed by a gradually slower increase of pore pressure. At this stage, some sensors show a quasi-steady state (see e.g. the sensor WA1 on top of Figure 6). Then, from a given time, the pore pressure is decreasing. Looking more in details, it is possible for most of the sensors to pinpoint quite accurately (in the order of a day) the peak of pore pressure, which characterises this transition (see the bottom part of Figures 6-7). For the borehole A2, the date 10/04/99 represents an average date for the peak occurrence. Note that the highest amplitude of the pore pressure decrease is observed on filter WA6 (located at 70 m from the second shaft axis), with a value of 0.08 MPa.

For the borehole B2, there is clearly a peak time-offset of 11 days depending on the sensor location: the peak is on the 29/03/99 for the closest sensor (WB1) to the second shaft (i.e. 60 m), and on the 11/04/99 for the far (i.e. 70 m) one (WB6), see bottom part of Figure 7. Note also that the amplitude of the pore pressure decrease is larger ( $\approx 0.2$  MPa) for the sensor closest to the second shaft. The previous two observations (time-offset and amplitude) would indicate that the phenomenon responsible for the pore pressure decrease is located closer from the filter WB1 than WB6.

Importantly, the above mentioned dates for the peak occurrence correlate very well with the date of the excavation works of the starting chambers. For instance, the first excavation phase of the North starting chamber started on 16/03/99 and was ended due to the occurrence of fracture surfaces (see 2.3) on 01/04/99, which is almost exactly the date at which the peak on WB1 is observed (29/03/99).

It is believed that such very good correlation is not a coincidence, which is strengthened by the observed axial symmetry of the main fractured surfaces with respect to the second shaft axis.

Finally, it is worth mentioning that in the Boom Clay, the pore pressure measurement technique using small piezometric filters such as in CLIPEX gives usually good results. In the case presented in section 2.4, the pore measurement was performed through a direct connection of the piezometric filter to a pressure transmitter (PTX 1400 from the company DRUCK), with a good accuracy (maximum error  $\pm 11$  kPa).

## 2.5 In-situ observation of the suction–fracturing relation

A relation between suction and fracturing has been observed recently during the installation of the RESEAL in-situ shaft seal test (Volckaert et al., in press). This experiment consists in the installation of a clay-based plug in a section of a small experimental shaft at the Mol URL (see Figure 8a), and in the following-up of its hydration and swelling. Prior installing this plug, three multi-piezometers were placed in the host-rock to measure in-situ water pressure as a function of the distance to the shaft wall (from 0.5 to 3.3 bar, see the left part of curves on Figure 8b). In a next step, the lining (concrete blocks and wooden plates) was removed and the backfill material was installed. From a mechanical point of view, this lining removal corresponds to a decrease of the radial total pressure from its equilibrium value to zero. Thus it is very similar to a gallery excavation, but only with a partial decompression as the initial radial pressure is already lower than the virgin in-situ one. The installation and the exploitation of this experiment allowed the following observations:

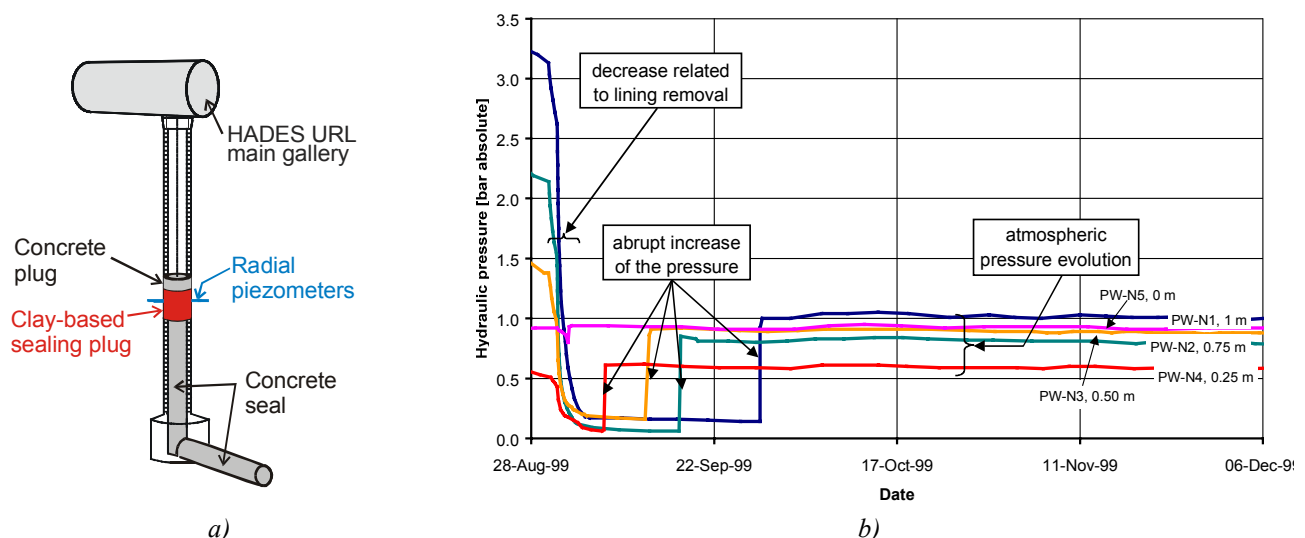


Fig. 8. The RESEAL in-situ seal test: a) design showing piezometers in the host-rock (Boom Clay) radially from the clay plug, b) hydraulic pressure measured on the North piezometer. Adapted after (Volckaert et al., in press).

- as the lining was removed to allow the placement of the backfill, fractures in the excavation wall of the small shaft were observed, i.e. in the Boom Clay;
- except the sensors located at the shaft wall that were at atmospheric pressure (see e.g. PW-N5), all the sensors showed a rapid decrease very well correlated in time with the lining removal, down to a minimum absolute pressure of about 0.1-0.2 bar (see Figure 8b). This low value of absolute pressure is interpreted as the pressure at which cavitation occurs locally at the instrument due to generation of suction. Thus, it is the in-situ confirmation that suction can generate around excavations in the Boom Clay only due to hydro-mechanical coupling;
- starting from the inner to the outer sensor, there is an abrupt increase of the pressure up to about 1.0 bar, i.e. atmospheric pressure. Note however that the sensor located at 0.25 m from the shaft wall (PW-N4 on Figure 8b) returns to its original value around 0.6 bar. In any case, this sudden re-equilibration of water pressure with atmospheric pressure is interpreted here as the opening of small fractures in the clay massif, which allows such a pressure re-equilibration. Note also that there is a time-offset (around 20 days) in this phenomenon: the sensor closest to the shaft wall re-equilibrates first (PW-N4 at 0.25 m from the wall, see Figure 8b), the sensor further to the shaft wall re-equilibrates last (PW-N1 at 1 m from the wall, see Figure 8b). This indicates a progressive generation of fractures in the Boom Clay outwards the excavation wall.

### 3. Predictions of the observed hydro-mechanical perturbations

Starting from the above-presented observations of pore pressure variation around excavations in the Boom Clay, it is checked in the following sections whether these observations can be predicted.

#### 3.1 Basics of the poromechanical formulation

The classical thermo-poromechanical framework of continuous media (Coussy, 1991) has been used successfully in reproducing and predicting the behaviour of the saturated Boom Clay (see e.g. Giraud, 1993; Picard, 1994; Sultan, 1997; Labiouse and Giraud, 1998). At the Mol site, the Boom Clay is characterised by a high porosity ( $n = 0.39$ ), a Biot's coefficient equal to unit ( $b = 1$ ) which is responsible for a strong hydro-mechanical coupling. Thus, under the assumption of elastic and plastic effective stresses, the following rate-form relations define the poroplastic isothermal isotropic behaviour for the Boom Clay

$$\underline{\dot{\sigma}}' = \underline{\dot{\sigma}} + \dot{u}_w \underline{I} = \underline{C}' : (\underline{\dot{\epsilon}} - \underline{\dot{\epsilon}}^p) \quad (1a)$$

$$\dot{u}_w = \frac{K_w}{n} \left( -tr(\underline{\dot{\epsilon}}) + \frac{\dot{m}}{\rho_w} - \dot{n}^p \right) \quad (1b)$$

where  $\underline{\sigma}'$  is the effective stress tensor,  $\underline{\sigma}$  the total stress tensor,  $u_w$  the pore pressure,  $\underline{I}$  the unit tensor,  $\underline{C}'$  the effective elastic matrix,  $\underline{\epsilon}$  the strain tensor,  $K_w$  the water bulk modulus,  $m$  the fluid mass content,  $n$  the porosity and superscript <sup>p</sup> standing for 'plastic part'. For the Boom Clay at the Mol site,  $\underline{C}'$  is computed from the effective elastic parameters  $E' = 300$  MPa,  $\nu' = 0.125$ . From these relations, the hydro-mechanical coupling can be seen clearly: the pore pressure enters the effective stress formulation which represents the H→M coupling, and the volumetric strain and plastic porosity enter the pore pressure formulation which represents the M→H coupling. The limit of the elastic domain is defined by the inequality

$$f(\underline{\sigma}, u_w, \zeta) < 0 \quad (2)$$

where  $f$  is the yield function and  $\zeta$  some history variable. For the Boom Clay, either a Mohr-Coulomb or a modified Cam-clay criterion usually allows to represent satisfactorily the observations, using the parameters  $c' = 300$  kPa,  $\phi' = 18^\circ$  or  $M = 0.81$ ,  $p_c = 6$  MPa (Labiouse and Giraud, 1998). For any state that violates the condition  $f \leq 0$ , the plastic strain rate  $\underline{\dot{\epsilon}}^p$  in (1a) is computed classically from a flow potential  $g$  following

$$\underline{\dot{\epsilon}}^p = \dot{\lambda} \frac{\partial g}{\partial \underline{\sigma}} \quad (3)$$

where the scalar  $\dot{\lambda}$  is obtained from the consistency condition during plastic flow.

#### 3.2 Instantaneous solutions

From a poroplastic framework similar to the one briefly presented in the previous section, Giraud (1993) and Labiouse and Giraud (1998) proposed an undrained solution to the excavation problem of infinite circular galleries. Worth pointing out that this solution gives an upper bound for the hydro-mechanical disturbances as the

Table 1. Parameters for the Boom Clay at the Mol site.

$E'$	300 MPa	$\psi$	$0^\circ-10^\circ$
$\nu'$	0.125	$b$	1
$c'$	300 kPa	$n$	0.39
$\phi'$	$18^\circ$	$K_w$	2 GPa

front support is neglected. Using the average parameters representative for the Boom Clay at the Mol site (see Table 1), these analytical solutions can be used to estimate the theoretical stress and pore pressure field around the second shaft, considering a full deconfinement in this case. With the realistic excavated radius of 4 m in the bottom part of the second shaft, the obtained fields (undrained solution) are presented on Figure 9. In this case, a plastic radius of 24.9 m is obtained with a wall convergence  $u_{ri} = 0.58$  m, and accordingly the undrained variation of pore pressure in the clay massif is nil for radii larger than this value, which is far from the observed variation mentioned in section 2.4. It is worth pointing out that negative pore pressures are generated (down to  $-1.2$  MPa) in the Boom Clay close to the excavation wall, only due to the elastic decompression (the plastic dilatancy is nil here as  $\psi = 0^\circ$ ).

We must examine the representativeness of the used parameters (given in Table 1). They represent a mean set of parameters determined from series of triaxial tests performed in different laboratories (Baldi et al., 1987; Horseman et al., 1987; Baldi et al., 1991; Mair et al., 1992). From these references, and depending on the interpretation, a lower effective friction angle can be obtained ( $\phi' \approx 14^\circ$ ) combined with a higher effective cohesion ( $c' \approx 550$  kPa). However, these modifications have not a significant overall effect on the results: all the other parameter remaining equal, the plastic radius extends to 20 m (compared to 24.9 m obtained in section 3.2) and  $u_{ri}$  to 0.41 m. Of course, if the lower bound for cohesion is considered (i.e.  $c' = 300$  kPa), an effective friction angle of around  $\phi' \approx 9.5^\circ$  would be required to fit the observation  $u_w = 0.2$  MPa at  $r = 60$  m, leading to a plastic radius of 74 m (i.e. almost  $20 \times r_i$ ). In this case, the convergence at the gallery wall would reach the very unrealistic value  $u_{ri} = 3.5$  m, whereas a maximum radial convergence of 14.5 cm has been measured on the lining (sliding ribs). Last, an upper bound for the plastic dilatancy angle ( $\psi = 10^\circ$ ) can be also be considered. With such a value, the undrained variation of pore pressure exhibits a higher gradient, which results in a smaller plastic radius of 16.5 m (see Figure 10) and wall convergence of  $u_{ri} = 0.25$  m.

In conclusion, it is not possible to conciliate the undrained solution using a single parameter set with the observations of the undrained pore pressure disturbance and realistic convergence values. It will be checked now whether fluid flow can explain this discrepancy.

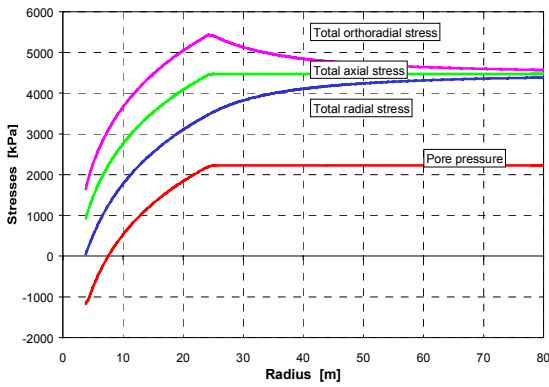


Fig.9. Total stress and pore pressure profile for an excavated radius of 4 m, and with  $\psi=0^\circ$ .

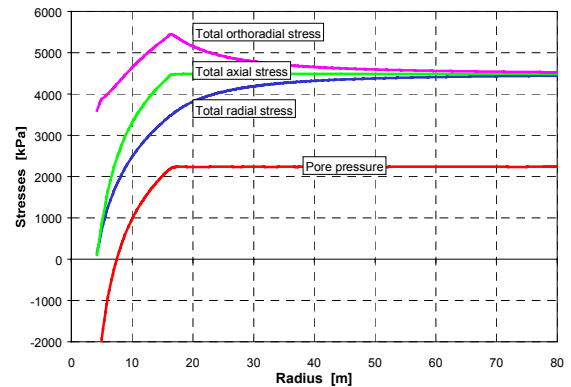


Fig.10. Total stress and pore pressure profile for an excavated radius of 4 m, and with  $\psi=10^\circ$

### 3.3 Time-evolution of the pore pressure field due to fluid flow

The solution presented above corresponds to the instantaneous solution, i.e. without any fluid flow. The evolution in time of this solution is mainly controlled by the fluid flow that will occur, which depends on the hydraulic boundary conditions, on the flow parameter and on the time considered. A first idea of these effects can be obtained by estimating the characteristic time for hydraulic diffusion  $\tau_h$  in the present case. Given the problem geometry,  $\tau_h$  is given by (see e.g. Giraud, 1993)

$$\tau_h = \frac{r_i^2}{k_h} \quad (4)$$

where  $r_i$  is the excavation radius and  $k_h$  the hydraulic diffusivity defined by

$$k_h = \frac{k}{\rho_w g} M \frac{3K' + 4G}{3K + 4G} \quad (5)$$

Using the parameters given in Table 1 for the Boom Clay, the value  $k_h = 1.21 \cdot 10^{-7} \text{ m}^2/\text{s}$  is obtained. Then, considering  $r_i = 4$  m (excavated radius), the characteristic time for hydraulic diffusion reads here  $\tau_h = 4.2$  year, which is much larger than the times involved in the phenomenon detailed in section 2.4. Thus, the hydraulic diffusion should not allow explaining the discrepancy between observations and

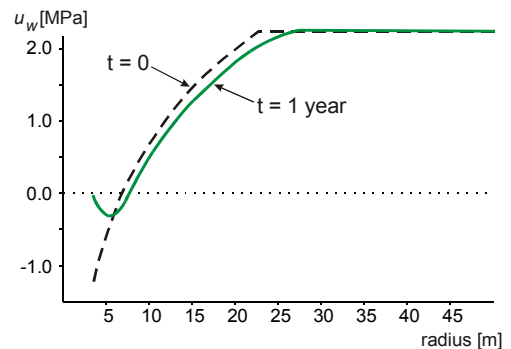


Fig.11. Evolution of the pore pressure profile from zero to one year (excavated radius = 4 m).

predictions. This can be confirmed by a HM calculation considering the case of a permeable boundary condition at the gallery wall (relevant as the lining permeability is several orders higher than the Boom Clay one). This boundary condition is then approximated by an imposed pressure  $u_w = 0$ , though in reality it is the relative humidity that is imposed. Using the Boom Clay hydraulic conductivity of  $4 \cdot 10^{-12}$  m/s, the obtained pore pressure profile after one year is reported on Figure 11 (thick line). Clearly, the drainage effect over a one year period does modify only slightly the pore pressure profile with respect to the instantaneous solution (dashed line on Figure 11). The fluid drainage towards the shaft does not reduce the observed discrepancy at radii of 60-70 m, thus other phenomena must be invoked.

### 3.4 Fracturing phenomena

If there is no fracturing in the host-rock, the key boundary condition is located at the shaft wall where the normal pressure  $\sigma_{n(w)}$  is close to zero (it is recalled that the second shaft and the starting chambers have been primarily lined with a soft lining with a low equilibrium pressure), see Figure 12a. Then, the classical solution presented in section 3.2 applies, giving a constant  $u_w$  at a radial distance of 60 m, as the plastic radius is close to 25 m.

However, fracturing occurred here under a very low  $\sigma_{n(w)}$  value. Worth mentioning that the fractures certainly do not extend far in the massif, the 25 m plastic radius obtained should represent the very maximum. In this case, the boundary condition  $\sigma_{n(w)} \sim 0$  is transferred (totally or partly) in the host-rock, more precisely at the fracture walls  $\sigma_{n(f)}$ . If the fractures are open, this new boundary condition reads  $\sigma_{n(f)} \sim 0$  (see Figure 12b), and it reduces the global radial stress  $\sigma_r$  in the fractured zone ( $\sigma_r \sim \sigma_{n(f)}$  holding for high fracturing density). This can be seen as an apparent increase of the excavated radius (see Figure 12b). This possible effect can be estimated performing the inverse calculation to obtain the theoretical excavated radius that would induce an undrained pore pressure variation of 0.2 MPa at 60 m (i.e. the observed one at borehole B2, see section 2.4). Here, a theoretical excavated radius of 10.7 m is obtained, with an associated plastic radius of 66.6 m (see Figure 13) and a wall convergence  $u_{ri} = 1.6$  m. Again this seems quite far from reality. This effect may have played a role in the observed variations of pore pressure, but certainly not to this extent, i.e. the apparent radius is probably lower than 10.7 m.

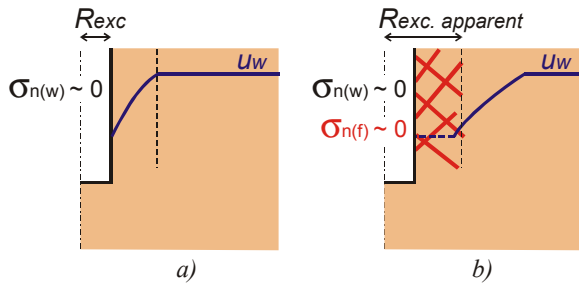


Fig.12. Schematic interpretation of the observed pore pressure variation associated with the second shaft excavation under low confinement: a) classical solution, b) solution with open fracturing.

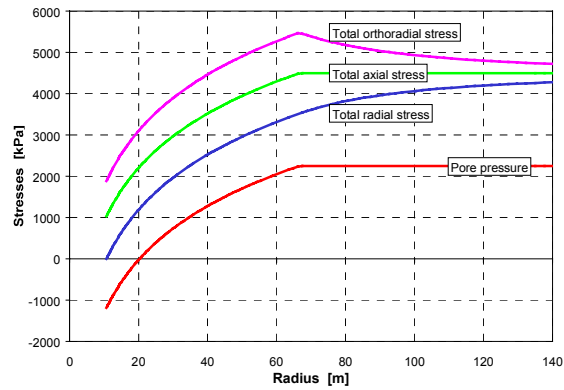


Fig.13. Total stress and pore pressure profile for an excavated radius of 10.7 m, and with  $\psi=0^\circ$ .

### 3.5 Time-evolution of the pore pressure field due to skeleton viscosity

At the scale representative for the present problem (excavated radius of around 4 m, pore pressure variation at a radius of 60 m), it has been shown in the previous section that the time-effects due to the fluid phase are negligible. We must check now whether the skeleton time-effects (viscosity) can be partly responsible of the observations. For the Boom Clay, the elasto-viscoplastic model with hardening-softening proposed by Rousset (1988) represents a reference one. Basically, it consists in a Bingham model i.e. a serie association between an elastic component and a viscoplastic one, the latter being a parallel association between a plastic component and a non-linear viscous one. However, this model was originally formulated and identified in total stresses, and it gives an elastic response at short-term which is not realistic (the plastic response is obtained as the limit case where the loading rate goes to zero).

Here, this model is generalised to poromechanics following Giraud (1993) and Djéran et al. (1994), and is extended to the more general framework of poro-elastoplasticity-viscoplasticity to obtain a coherent short-term response (the plastic response is obtained as the limit case where the loading rate is infinitely large). Accordingly, the total strain rate is partitioned between an instantaneous component (elastoplastic) and a differed one (viscoplastic), i.e.

$$\dot{\underline{\epsilon}} = \dot{\underline{\epsilon}}^e + \dot{\underline{\epsilon}}^p + \dot{\underline{\epsilon}}^{vp} \quad (6)$$

The non-linear viscoplastic strain rate is defined from the generalised Perzyna viscoplasticity (1966) following

$$\dot{\underline{\epsilon}}^{vp} = \frac{1}{\eta} \left\langle f^{vp}(\underline{\sigma}', \alpha) \right\rangle^n \frac{\partial g^{vp}}{\partial \underline{\sigma}'} \quad (7)$$

where  $\eta$  is the viscosity coefficient,  $n$  the viscosity exponent,  $f^{vp}$  the viscoplastic criterion (Mohr-Coulomb here),  $g^{vp}$  the viscoplastic flow potential (Von Mises), and  $\alpha$  the hardening variable defined from the principal irreversible (plastic and viscoplastic) strain through

$$\alpha = \frac{1}{2} \int_0^t \sum |\dot{\epsilon}_i^{irr}| dt \quad (8)$$

Here the assumption is made that the cohesion of the viscoplastic criterion  $c^{vp}$  is related to  $\alpha$  following

$$c^{vp} = \begin{cases} \frac{\alpha}{\epsilon_0} c_{peak} & \text{if } 0 \leq \alpha \leq \epsilon_0 \\ c_{peak} & \text{if } \epsilon_0 \leq \alpha \leq \epsilon_1 \\ c_{peak} + \frac{\alpha - \epsilon_1}{\epsilon_2 - \epsilon_1} (c_{res} - c_{peak}) & \text{if } \epsilon_1 \leq \alpha \leq \epsilon_2 \\ c_{res} & \text{if } \epsilon_2 \leq \alpha \end{cases} \quad (9)$$

where  $\epsilon_0$ ,  $\epsilon_1$  and  $\epsilon_2$  are hardening parameters. The viscoplastic parameters retained here are taken from (Djéran et al., 1994) and are reported in Table 2. Finally, one can estimate the viscous characteristic time  $\tau_\eta$  for the non-linear viscosity  $\eta$  by the relation (note that  $\tau_\eta$  does not depend from a length)

$$\tau_\eta = \frac{\eta}{G} \tilde{\sigma}^{(1-n)} \quad (10)$$

where  $\tilde{\sigma}$  is a reference stress. Considering the value  $\tilde{\sigma} = 4.5$  MPa (mean stress at 225 m depth) and the viscous exponent  $n = 4$  leads to the value  $\tau_\eta \approx 10$  day, which is about two orders of magnitude lower than the characteristic hydraulic time  $\tau_h$  given by equation (4) at the present scale. Therefore, we can expect the viscous effects to be more important than the ones induced by water flow. The numerical solution is computed with the viscoplastic parameters given in (Djéran et al., 1994) and reported in Table 2, using an explicit finite difference method. An axisymmetric one-dimensional instantaneous (no creep and fluid flow) excavation is considered, until an internal pressure of two bars at the shaft wall. From this stage, time-dependent effects (creep and fluid flow) are then computed with the condition  $u_w = 0$  at the shaft wall (same approximation than in section 3.2). After a given time (zero day for case A, seven days for case B), the internal pressure is replaced by a fully rigid confinement (prescribed nil radial displacements). Starting from the instantaneous elastoplastic solution with a plastic radius of about 25 m (see section 3.2), there is a significant variation of pore pressure resulting from the mean pressure redistribution. The sign of this variation depends on the radial position  $r$ : close to the shaft wall ( $r_i < r < 20$  m) the pore pressure increases mainly due to the viscoplastic recompression on the lining, whereas far in the massif ( $r > 20$  m) the pore pressure decreases due to the viscoplastic decompression (see Figures 14a-b). Note that for case B, the pore pressure drop at 60 m radius is around the observed value of 0.2 MPa (Figure 14b). Obviously, these results must be considered with some care, as the excavation process and geometry are extremely simplified here. Last, it must be pointed out that the wall convergence remains constant ( $u_{r_i} = 0.58$  m) in case A, but increases during the first seven days in case B to  $u_{r_i} = 2.16$  m, which again represents a quite large value.

Table 2. Boom Clay parameters for the viscoplastic part of the model (from Djéran et al, 1994).

$\phi^{vp}$	4°
$c_{peak}$	0.12 MPa
$c_{res}$	0.03 MPa
$\epsilon_0$	2.5%
$\epsilon_1$	3.5%
$\epsilon_2$	5.0%
$\eta$	300 MPa <sup>4</sup> ·day
$n$	4

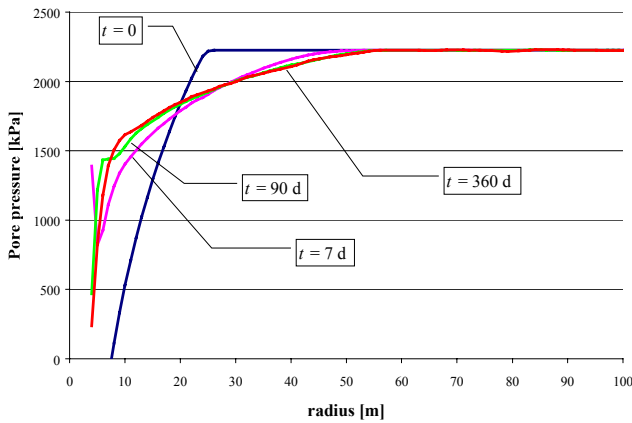


Figure 14a. Time-evolution of the pore pressure predicted in poro-elastoplasticity-viscoplasticity, for case A.

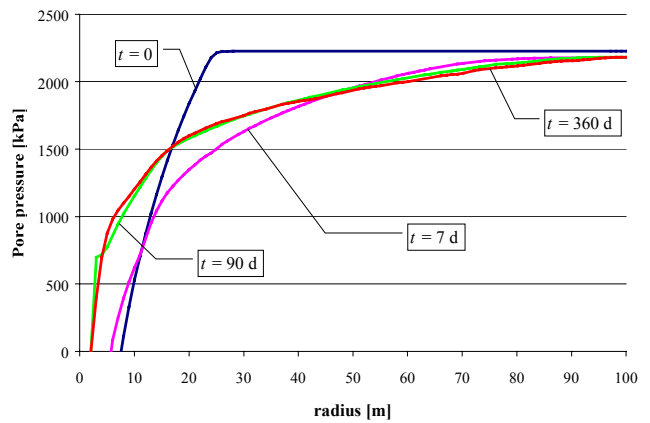


Figure 14b. Time-evolution of the pore pressure predicted in poro-elastoplasticity-viscoplasticity, for case B.

To conclude, viscous effects can certainly be invoked to explain part of the observations, though their realistic quantification would deserve a more detailed study. An important point could be the comparison between the computed wall convergence and the real one; for technical reasons, the latter could not be measured around the second shaft. However, it is worth pointing out that, on a qualitative viewpoint, the viscous effects do extend the perturbation in the massif by decreasing the mean pressure gradient, which is consistent with the observations.

#### 4. Conclusion

As detailed previously, it is not straightforward to obtain a coherent interpretation of the available observations made around the excavations in the Boom Clay at the Mol site, due to the numerous effects that can superimpose. Combining the observations of fracturing (sections 2.2, 2.3 and 2.5), the large extent of the observed pore pressure variation (section 2.4), and the hydro-mechanical predictions given in section 3, we interpret that the observations presented here as a combination of two factors:

- the very low support pressure imposed by the soft lining, which induced a quasi-instantaneous-like response of the massif (the extent of the hydraulic perturbation of this factor can be expected around 25 m);
- the large time on which this low support condition was active, which favoured the occurrence of differed effects. These effects originate mainly from the skeleton viscosity of the Boom Clay as the time effects due to fluid flow are negligible.

These two factors have resulted in an increase of the initial decompression of the clay massif:

- in the near field, and due to the negative pore pressure that developed in this zone as a result of the strong hydro-mechanical coupling, it led to fracturing. If partly open, they may have resulted in an increase of the apparent radius of the excavation (see Figure 12). Interestingly, a similar relation between pore pressure and fracturing has been observed in undrained test performed on initially saturated sand materials. In these tests, the shear strain localisation is associated with the occurrence of suction (Desrues, 1999). At least two indications corroborate this idea: the negative pore pressures that are theoretically predicted around excavations in the Boom Clay (see Figures 9-10), and the suction-fracturing relation that is evidenced in the RESEAL test (see section 2.5);
- in the far field, it led to a more gentle decompression of the clay massif, which due to the HM coupling and the relative compressibility of the pore water with respect to the clay, induced a slight decrease of the pore water pressure such as observed on the CLIPEX piezometers. The accurate quantification of these effects should of course rely on well calibrated model parameters, such as the viscosity coefficient and the volumetric part of the viscoplastic behaviour.

Finally, we must be careful with this interpretation as it cannot be proved firmly. One reason for that is the discrete nature of fracturing, which makes it difficult to define a homogeneous equivalent media and which brings questions about the validity of the continuous media framework used. A second reason comes from the one-dimensional assumption made for all the computations presented here, which does not allow to consider properly the excavation sequence and timing.

To validate/invalidate the proposed interpretation, new observations and data are required, and they will become available soon. A characterisation of the fractured zone will be performed before the end 2000 by means of cored-drilling(s) and seismic investigation using the BGR mini-sonic probe (see Alheid et al., 1999), possibly associated with accurate cross-hole measurements. Also, the CLIPEX project will allow (mid-2001) to record the perturbations generated by the excavation of a gallery between the second shaft and the existing Test-Drift (see Figure 1): field observation of possible fracturing, generation of suction close to the excavation front and possible fracturing evidenced by abrupt re-equilibration to atmospheric pressure.

Worth mentioning that, due to the viscous behaviour of the Boom Clay, the effect of a potential fracturing on the overall performance of a high level radioactive waste repository should remain limited due to self-healing effects, though this point certainly deserves further research. That is already partly foreseen in the continuation of the RESEAL project.

#### Acknowledgements

The European Commission is greatly acknowledged for funding of the CLIPEX and RESEAL projects, together with the following respective partners: ANDRA, ENRESA, EIG PRACLAY for the CLIPEX project; ANDRA, ENRESA and ONDRAF for the RESEAL project.

## References

- Alheid H.J., Knecht M., Boisson J.Y., Homand-Etienne F. and Pepa S. 1999. Comparison of in-situ hydraulic and seismic measurements in the excavation damaged zone of underground drifts. *Proceedings of the 9<sup>th</sup> International Congress on Rock Mechanics, Paris*, Vouille & Berest (eds), Balkema, Vol 2: 1263-1266.
- Baldi G., Borsetto M. and Hueckel T. 1987. Calibration of mathematical models for simulation of thermal, seepage and mechanical behaviour of Boom Clay. *Commission of the European Communities, Nuclear Science and Technology, EUR 10924*.
- Baldi G., Hueckel T., Peano A. and Pellegrini R. 1991. Developments in modelling of the thermo-hydro-geomechanical behaviour of Boom clay and clay-based buffer materials. *Commission of the European Communities, Nuclear Science and Technology, EUR 13365*.
- Barnichon J.D. 1998. Contribution of the bounding surface plasticity to the simulation of gallery excavation in plastic clays. *5<sup>th</sup> International Workshop on Key Issues in Waste Isolation Research*, Barcelona, Dec 2-4.
- Bernier F. and Van Cauteren L. 1998. Instrumentation programme near the face of an advancing tunnel in Boom Clay. *The Geotechnics of Hard Soils - Soft Rocks*, Evangelista & Picarelli (eds), Balkema, Rotterdam: 953-959.
- Bonne A., Beckers H., Beaufays R., Buyens M., Coursier J., De Bruyn D., Fonteyne A., Genicot J., Lamy D., Meynendonckx P., Monsecour M., Neerdael B., Noynaert L., Voet M. and Volckaert G. 1992. The HADES demonstration and pilot project on radioactive waste disposal in clay formation. *Commission of the European Communities, Report EUR 13851*.
- Coussy O. 1991. Mécanique des milieux poreux. *Editions Technip, Paris*, 437 pp.
- Djéran I., Bazargan B., Giraud A. and Rousset G. 1994. Etude expérimentale du comportement thermo-hydro-mécanique de l'argile de Boom. *G3S, Rapport final n°94-002, contrat ONDRAF-G3S*.
- Desrues J. 1999. Oral communication at the 2<sup>nd</sup> Euroconference on Rock Physics and Rock Mechanics, Edinburgh, November.
- Giraud A. 1993. Couplages thermo-hydro-mécaniques dans les milieux poreux peu perméables : application aux argiles profondes. *Thèse de Doctorat de l'Ecole Nationale des Ponts et Chaussées*, 269 pp.
- Horseman S.T., Winter M.G. and Entwistle D.C. 1987. Geotechnical characterization of boom clay in relation to the disposal of radioactive waste. *Commission of the European Communities, Report EUR 10987*.
- Labieuse V. and Giraud A. 1998. Analytical solutions for the undrained response of a poro-elasto-plastic medium around a cylindrical opening. *Poromechanics, Thimus et al. (eds), 1998 Balkema, Rotterdam*: 439-444.
- Mair R.J., Taylor R.N. and Clarke B.G. 1992. Repository tunnel construction in deep clay formations. *Commission of the European Communities, Report EUR 13964*.
- Perzyna P. 1966. Fundamental problems in viscoplasticity. *Advances in Applied Mechanics*, Vol 9: 243-377.
- Picard J.M. 1994. Ecouissage thermique des argiles saturées : application au stockage de déchets radioactifs. *Thèse de Doctorat de l'Ecole Nationale des Ponts et Chaussées*, 283 pp.
- Rousset G. 1988. Comportement mécanique des argiles profondes – Application au stockage de déchets radioactifs. *Thèse de Doctorat de l'Ecole Nationale des Ponts et Chaussées*, 435 pp.
- Sultan N. 1997. Etude du comportement thermo-mécanique de l'Argile de Boom : expériences et modélisations. *Thèse de Doctorat de l'Ecole Nationale des Ponts et Chaussées*, 310 pp.
- Volckaert G., Dereeper B., Put M., Ortiz L., Gens A., Vaunat J., Villar M.V., Martin P.L., Imbert C., Lassabatère T., Mouche E. and Cany F. In press. A large scale in-situ demonstration test for repository sealing in an argillaceous host-rock (the RESEAL project). *Contract N° FI4W-CT96-0025, Final report phase 1*.